Journal of Materials Chemistry C

Accepted Manuscript

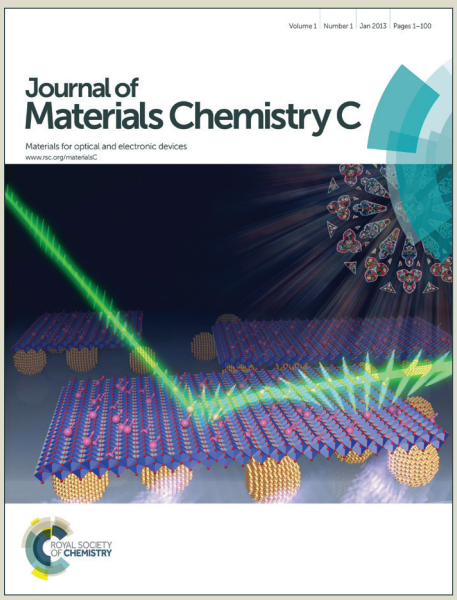

ROYAL SOCIETY OF CHEMISTRY

www.rsc.org/materialsC

Cite this: DOI: 10.1039/c0xx00000x

www.rsc.org/xxxxxx

ARTICLE TYPE

A Hybrid White Organic Light-Emitting Diode with Above 20% External Quantum Efficiency and Extremly Low Efficiency Roll-Off

Ning Sun, Qi Wang, Yongbiao Zhao, Dezhi Yang, Fangchao Zhao, Jiangshan Chen, Dongge Ma*

Received (in XXX, XXX) Xth XXXXXXXXX 20XX, Accepted Xth XXXXXXXXX 20XX
DOI: 10.1039/b000000x

Recently, the combination of blue fluorescent emitter with long wavelength phosphorescent emitters in so-called hybrid white organic light-emitting diodes (WOLEDs) has attracted much attention. However, as compared to the previously reported all-phosphor WOLEDs, the efficiencies of hybrid WOLEDs are yet unsatisfactory. In this work, through a delicate design of the device structure, nearly all generated excitons are harnessed for light emission in hybrid WOLED. The hybrid device shows excellent electroluminescence (EL) performance with forward-viewing maximum external quantum efficiency (EQE), current efficiency (CE) and power efficiency (PE) of 21.2%, 49.6 cd A^{-1} and 40.7 lm W^{-1}, respectively then slightly decreases to 20.0%, 49.5 cd A^{-1} and 37.1 lm W^{-1} at 1000 cd m^{-2}, which are the highest levels reported so far. This work provides an avenue for the development of blue fluorescent emitter together with a novel device structure design for ultrahigh performance hybrid WOLEDs in the future.

1. Introduction

White organic light-emitting diodes (WOLEDs) have drawn substantial attentions due to their great potential in the fields of solid-state lightings and flat-panel displays. Much work has been carried out to improve the efficiency of WOLEDs.[1] Almost highly efficient WOLEDs are based on fully phosphorescent structures because they can achieve up to 100% internal quantum efficiency (IQE) by efficiently harvesting both singlet and triplet excitons. However, the development of all phosphorescent WOLEDs is severely limited by the absence of efficient deep-blue phosphorescent emitters with operational lifetimes suitable for commercial applications. Thus, the combination of a highly stable blue fluorophor with red and green phosphors in a so-called hybrid WOLED provides an alternative to resolve this problem.

The blue-light source is employed to overcome the color-stability limitations found for all-phosphor-doped WOLEDs. The hybrid WOLED can simultaneously take the advantages of good stability of the blue fluorophore and high efficiency of the long wavelength phosphors. So the structures based on a hybrid system are a better option for researchers with the aim to commercialize WOLEDs. In general, hybrid WOLEDs can be achieved by incorporating either two complementary colors (blue and yellow or orange) or three primary colors (blue, green, and red) in two architectures, including a single-emissive-layer (single-EML),[2] or multi-emissive-layers (multi-EML).[3,4]

In the single-EML structure, the phosphors (green/red/orange/yellow) are doped into a blue fluorophor to form the EML. Therefore, the blue fluorophor should not only possess efficient blue fluorescence, but also acts as host for the phosphors, which dominates the main emission mechanism and directly affects the external quantum efficiency (EQE) of the device. The main problem in such single-EML hybrid WOLEDs is the lack of suitable fluorescent blue emitter which has to meet strict requirements including high photoluminescent quantum yield (PLQY), high triplet energy, bipolar property, and good thermal stability. In addition, to attain sufficient blue emission from direct radiative singlet excitons decay on blue fluorophor, phosphor concentration has to be very low to suppress singlet excitons transfer from blue fluorophor to phosphor by Förster transfer or diffusion. The extremely low doping concentration required (ca. 0.1%) to achieve white-light emission is quite difficult to control and to reproduce in the co-evaporation process. Compared with the multi-EML white device, the single-EML device shows a pronounced efficiency roll-off at high current densities, which is probably caused by incomplete triplet utilization due to the low doping concentration, representing another drawback. For the multi-EML structure, the requirements of blue fluorescent emitter are not strict as that in the single-EML structure. And the multi-EML structure can afford more flexibility for the manipulation of each emissive layer as well as precise control of the exciton distributions or charges in different EMLs, providing a reliable strategy to fabricate hybrid WOLEDs. Owing to the incomplete coverage of whole visible region, two complementary color strategy suffers from a rather low color-rendering index (CRI), which is insufficient for illumination

sources, making them a less attractive approach for generating white light with a high color quality.

Thus, it is necessary to incorporate three primary colors in a multi-EML structure in order to achieve high performance of hybrid WOLEDs. Many studies have been reported based on such strategy.[4] The commonly used device architecture of hybrid WOLEDs is the fluorescence-interlayer-phosphorescences,[3,4] in which the fluorophor close to the exciton generation zone to catch the singlet excitons, and the phosphors farther away, fed by the diffusing triplet excitons. Due to the low triplet energy level of blue fluorophor, the interlayer with high triplet energy is indispensable to insert between the two kinds of dyes, preventing phosphorescence quenching. But partial triplet excitons generated in the exciton generation zone can be quenched by the blue fluorophor, leading to parasitic exciton losses such that the device can not realize 100% exciton harvesting. This means that such devices cannot realize a theoretical IQE of 100% which corresponds to ~20% to 22% forward-viewing EQE.[5] It also explains the low forward-viewing EQEs obtained in these reports, which are far below 20%.

With further development of blue fluorescent emitters, some reports focused on hybrid WOLEDs were intended for achieving a theoretical forward-viewing maximum EQE of ~20% to 22%. For example, Schwartz et al. introduced a new blue fluorophor (4P-NPD) whose triplet energy falls in between $Ir(MDQ)_2(acac)$ and $Ir(ppy)_3$.[6] To obtain simultaneous emissions from the blue fluorescence and orange phosphorescence in the same layer, the orange phosphor $Ir(MDQ)_2(acac)$, which was supposed to harvest the triplet excitons, was directly doped into the 4P-NPD layer with extremely low concentration. The interlayer was incorporated to suppress the quenching processes between 4P-NPD and $Ir(ppy)_3$. Nevertheless, the forward-viewing EQE was only 11.2% at 1000 cd m^{-2}, still far from the theoretically forward-viewing maximum EQE of ~20% to 22%. Although the PLQY of each emitter is reasonable high, the combination suffered from efficiency losses due to the incomplete triplet exciton transfer to $Ir(MDQ)_2(acac)$, or induced by the interlayer. The rough structure design of device constrains the practical efficiency, which makes 4P-NPD receive less attention. Since then barely any hybrid WOLEDs based on 4P-NPD has been reported, and research efforts shifted to synthesis of blue fluorophor with sufficient high triplet energy (>2.4 eV) to allow the sensitization of commonly used green phosphors.[3a,4d,7] Among this class of blue fluorophores being investigated, DPMC and DAPSF reported by Xiao-Hong Zhang and Chun-Sing Lee et al. were highly attractive because they exhibited very high maximum total EQEs of 21.0% and 20.2% in the optimized hybrid WOLEDs.[7] However, considering the fact that total efficiency~1.7*forward-viewing efficiency,[8] the corresponding forward-viewing maximum EQEs were decreased to 12.8% and 11.9%. Let alone the poor quality of white light, the low efficiencies should be mainly attributed to both blue fluorescent emitters with their intrinsically unsatisfactory PLQYs (79% and 74%) which are important prerequisite to obtaining high EQEs. Most recently, we advanced conventional hybrid WOLED structure by eliminating the interlayer between the fluorescent and phosphorescent regions, achieving a record forward-viewing maximum EQE of 19.0% which is close to theoretically maximum value of ~20% to 22%.[9] However, the intrinsic defect of device structure restricts the possibility for 100% exciton harvesting for light emission. The energy transfer from $Ir(ppy)_2(acac)$ to the nonradiative triplet state of 4P-NPD cannot be completely avoided due to the mismatched triplet energy levels of both dyes, such that it could not be further improved to obtain forward-viewing EQE above 20%.

Therefore, it is highly desirable to develop newly effective device that can render various channels to harvest all excitons together with a reduced efficiency roll-off. In this work, we propose a new device design strategy to achieve an hybrid WOLED with EQE above 20% by elaborately arrangement of three primary-color EMLs. The key feature of our novel structure is employing CBP as the host for all EMLs. By virtue of the bipolar transport properties of CBP, both charge carriers can transport into every EMLs, providing more flexibility for the arrangement of three (primary-color) EMLs, and hence successfully separating dyes with mismatched triplet energy levels which provides possibility to achieve nearly 100% exciton harvesting. The hybrid device shows excellent EL performance with forward-viewing maximum EQE of 21.2%, and less pronounced efficiency roll-off, yet, at an illumination-relevant brightness of 1000 cd m^{-2}, the EQE can reach 20.0%. Remarkably, at the brightness of 5000 cd m^{-2} and 10000 cd m^{-2}, the EQEs are still as high as 17.8% and 16.2%.

2. Experimental

Materials

PEDOT: PSS (AI4083) was purchased from Heraeus Ltd. Cs_2CO_3 was purchased from Sigma-Aldrich. All other organic materials were purchased from Nichem Fine Technology Co. Ltd. These materials were used as received.

Device fabrication

The fabricated devices were grown on clean glass substrates pre-coated with a 180 nm thick layer of indium tin oxide (ITO) having a sheet resistance of 10 Ω square^{-1}. The ITO surface was treated by oxygen plasma for 2 min, following a degrease in an ultrasonic solvent bath, then it was dried at 120 ^{0}C. A layer of PEDOT:PSS was spin-coated onto the precleaned ITO substrates, and then baked at 120 °C in a vacuum oven for 30 min to extract residual water. All other layers were grown in succession by thermal evaporation without breaking vacuum (~5×10^{-4} Pa).

Measurements

Current–voltage–brightness characteristics were measured by using a Keithley source measurement unit (Keithley 2400 and Keithley 2000) with a calibrated silicon photodiode. The EL spectra were measured by a Spectrascan PR650 spectrophotometer. All the measurements were carried out in ambient atmosphere.

3. Results and Discussion

3.1 Selection of the materials

Except for rational device engineering, high-efficient dyes are another crucial factor to promote device efficiency, so the starting point for constructing the hybrid WOLED demonstrated below was the selection of lumophores. For a three primary-color system, the individual emission spectra of emitters should compensate each other so that the white spectrum generated can cover the entire visible region. One crucial factor for harvesting all the excitons generated in device is that the triplet state energy of blue fluorophor should be above at least one phosphorescent emitter. Therefore, the selection of the blue fluorescent emitter is key to the success of achieving theoretical forward-viewing maximum EQE of ~20% to 22%. There are not many choices but to use *N*,*N*′-di-1-naphthalenyl-*N*,*N*′-diphenyl-[1,1′:4′,1″:4″,1‴-quaterphenyl]-4,4‴-diamine (4P-NPD), a deep-blue emitter with a dominant emission peak at 425 nm, due to its high triplet energy level (2.3 eV) and high PLQY (92%).[6] The commonly used fac-tris(2-phenylpyridine) iridium ($Ir(ppy)_3$) and iridium(III)bis(2-methyldibenzo[*f*,*h*]quinoxaline)(acetylacetonate) ($Ir(MDQ)_2(acac)$) were chosen as the phosphorescent green and orange dopants, respectively. In order to reduce structural heterogeneity and facilitate charge transport between different emissive centers, all lumophores were doped into a single, common conductive host, 4,4′-bis(N-carbazolyl)biphenyl (CBP). 4,4′,4″-tri(N-carbazolyl)triphenylamine (TCTA) with high-lying lowest unoccupied molecular orbital (LUMO) and 1,3,5-tri(m-pyrid-3-yl-phenyl)benzene (TmPyPb) with low-lying highest unoccupied molecular orbital (HOMO), serving as electron-blocking layer (EBL) and hole-blocking layer (HBL) respectively, were employed adjacent to the EMLs. And their high triplet energy levels can also confine excitons efficiently in EMLs. A 4% cesium carbonate (Cs_2CO_3) doped with TmPyPb was used as the n-ETL to achieve a low driving voltage. A Cs_2CO_3/Al acted as a bilayer cathode. Meanwhile, PEDOT:PSS provided an intermediate energy level to facilitate hole injection from the indium tin oxide (ITO) anode to the hole transport layer (HTL), N,N′-diphenyl-N,N′-bis(1-naphthyl)-(1,1′-biphenyl)-4,4′-diamine (NPB).

3.2 Design and fabrication of nearly 100% exciton harvesting architecture

The motivation of the design concept is to achieve nearly 100% IQE. The important requirement for that aim is the utilization of all generated excitons, that is, both singlet and triplet excitons should be employed for emission. However, except for the employment of efficient materials, combination with elaborate device engineering is also necessary. In this section, considering the intrinsic properties of emitters, we rationally arrange the sequence of three (primary color) EMLs of the multi-EML hybrid WOLED, enabling the device with 100% for the IQE.

Though 4P-NPD exhibits high PLQY, such emitter possess relatively low triplet state energy (2.3 eV) compared to $Ir(ppy)_3$ (2.4 eV), and thus it is not ideally suitable for locating it adjacent to the $Ir(ppy)_3$ containing layer in hybrid WOLEDs.[6,10] This problem can be solved by inserting other layers between the two emitting regions, which can prevent the transfer of emissive triplet excitons from $Ir(ppy)_3$ to the non-emissive ones of 4P-NPD. Here, we used CBP:$Ir(MDQ)_2(acac)$ as the red EML to separate the mismatched green and blue EMLs. From the relationship of the triplet energy levels, it is obvious that the triplet excitons on 4P-NPD can well be harvested by $Ir(MDQ)_2(acac)$. However, the singlet excitons in the blue EML can also direct transfer via Förster transfer, or diffuse and subsequent Förster transfer, to the CBP:$Ir(MDQ)_2(acac)$ layer, contributing to the red emission, such that no white emission is possible. Considering the fact that the singlet exciton has a shorter diffusion length than the triplet exciton, which is originating from their different lifetimes,[11] it provides possibility to separate them spatially. More precisely, the red EML should be placed at a distance larger than the singlet exciton diffusion length but shorter than the triplet exciton diffusion length. On the one hand, it allows for sufficient blue emission for generating white light by carefully controlling the blue EML thickness. On the other hand, the non-emissive triplet excitons of 4P-NPD can easily diffuse into the CBP:$Ir(MDQ)_2(acac)$ layer where they can excite the orange phosphor $Ir(MDQ)_2(acac)$ to generate red emission. Therefore, all triplet excitons on 4P-NPD are transferred to the triplet energy of orange phosphor $Ir(MDQ)_2(acac)$, which can decay radiatively, potentially without losses, while maintaining the singlet energy exclusively on the blue fluorophore.

Different from conventional structures with only one narrow region for exciton generation and recombination due to the utilization of the unipolar electron- or hole-transport host materials, the bipolar transport properties of CBP serving as the host in the novel structure provide a means to simultaneously excite blue and green emitters at spatially separated positions. Since the hole mobility of CBP is nearly one order of magnitude higher than its electron counterpart,[12] it can be assumed that more excitons would generate near the interface between EML/HBL. Because the intensity of light emitting from phosphorescent dyes is generally higher than that from fluorescent ones, the blue EML should be positioned facing the cathode side in order to achieve a balance of the blue emission with the red and green emissions.[13] So the green EML located at the other side of the EML, near the EBL. As known, triplet excitons have large diffusion length (tens of nm) due to their intrinsically long lifetime.[11] The excess red emission due to the exciton transfer from green EML would impair the balance of spectrum. The pure CBP interlayer should be introduced between the red and green regions to prevent the unwanted energy transfer, resulting in a desired output color balance. Based on these considerations, we arranged the novel structure of the EML with a G–Interlayer–R–B sequence from the anode to the cathode (see Figure 1). Overall, all generated excitons are consumed for white emission. The singlet excitons generated on the blue fluorophor can be used for blue emission, and the triplet excitons consume for the phosphorescent emission, realizing nearly 100% exciton harvesting.

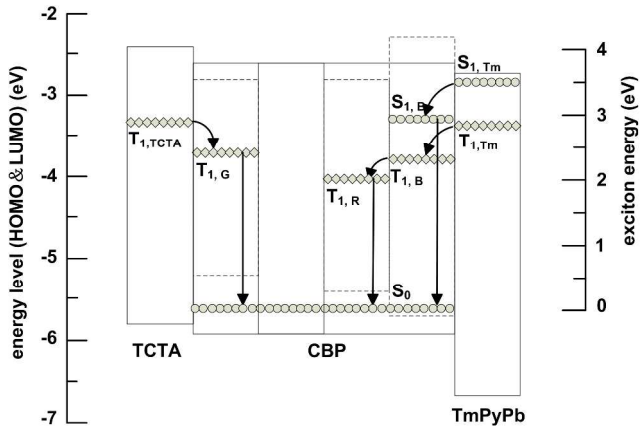

Figure 1. Energy level scheme for materials used in the hybrid WOLED, and exciton (S_0, S_1, and T_1) energy diagram of the emitter layers. R, G, Band Tm represents $Ir(MDQ)_2(acac)$, $Ir(ppy)_3(acac)$, 4P-NPD and TmPyPb, respectively.

3.3 Device performance

After optimization of the concentrations of guest emitters as well as the thicknesses of EMLs and adjacent functional layers, the hybrid device exhibits very impressive EL performance with a turn-on voltage of 3.3 V (see Figure 2). A forward-viewing maximum EQE of 21.2% is achieved at a current density 0.27 mA cm^{-2}, and remains to be 20.0% at a practical brightness of 1000 cd m^{-2}. Assuming an optical outcoupling efficiency of roughly ~20% to 22%, this corresponds to an IQE close to unity, which means a full conversion of the electrically generated excitons into light. This device gives a forward-viewing maximum power efficiency (PE) and current efficiency (CE) of 40.7 lm W^{-1} and 49.6 cd A^{-1}, then slightly decrease to 37.1 lm W^{-1} and 49.5 cd A^{-1} at 1000 cd m^{-2}. Remarkably, at the brightness of 5000 cd m^{-2} and 10000 cd m^{-2}, the EQEs are still as high as 17.8% and 16.2%. Although both 40.7 lm W^{-1} and 37.1 lmW^{-1} are the highest PEs ever reported for hybrid WOLEDs compared to their own counterparts. Considering the recorded EQEs exceeding 20% and the correlation between PE and EQE,[14] the PEs are unsatisfactory that should be attributed to the high driving voltage. For example, the driving voltage at 1000 cd m^{-2} is as high as 4.2 V, which is much higher than counterparts' values.[2c,3a,4c,7] When CBP used as the host material for emitters, high driving voltages were often observed for the devices due to its low electron drift mobility.[15] This problem will be most likely overcome with the development of ambipolar host material which allows for high mobilities of both electrons and holes, ultimately leading to a rather high PE.

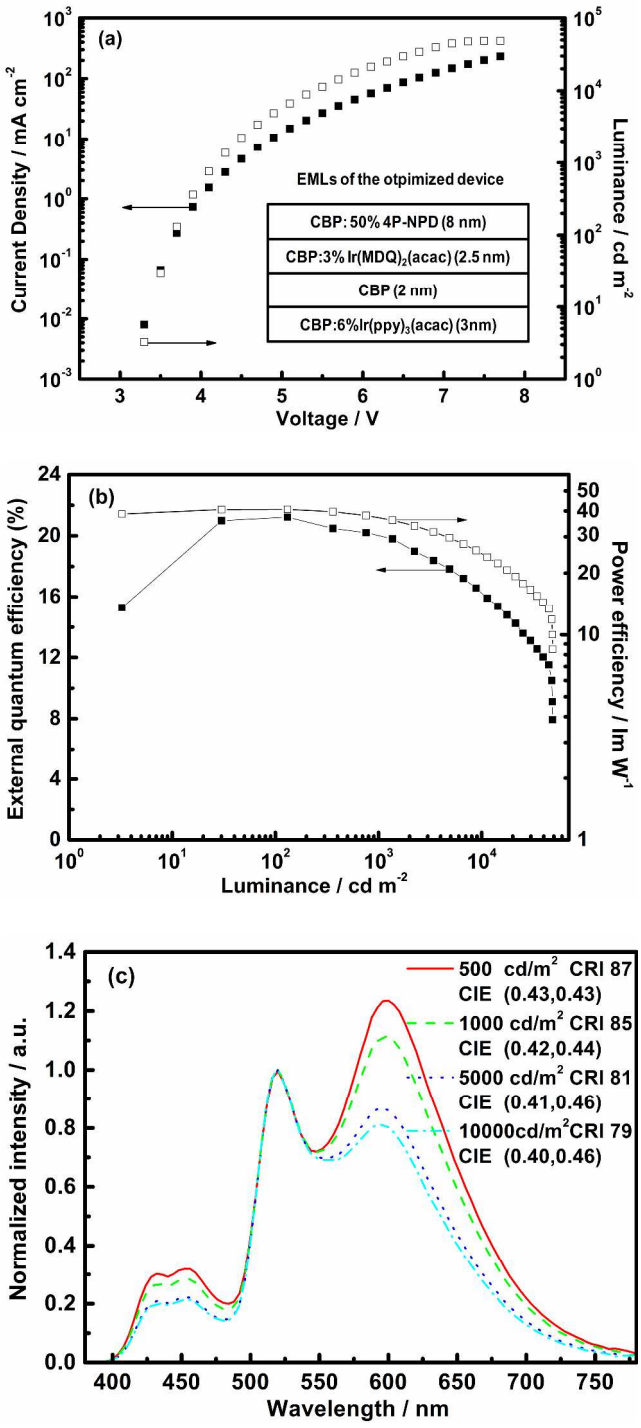

Figure 2. (a): Current density–luminance–voltage characteristics, with luminance measured in forward direction without outcoupling enhancement techniques. The inset shows the components of the EMLs. (b): External quantum efficiency and power efficiency versus luminance characteristics of the optimized device. (c): Normalized EL spectra at different brightness levels.

In addition to the realization of high efficiency, currently issue on efficiency roll-off is well resolved in this hybrid device. The critical current density j_c, where EQE declines by half from its peak,[16] is about 174 mA cm^{-2}, which is comparable to or even

higher than some of the high-performance single- or multi-EML WOLEDs demonstrated before.[4a,17] The reasons for such low efficiency roll-off will be discussed in the following section. Our device can also afford a high-quality white light with a high CRI of 85 at 1000 cd m^{-2}, Commission Internationale de L'Eclairage (CIE) coordinates of (0.42,0.44) and a correlated color temperature (CCT) about 3544 K, corresponding to a desirable warm white illumination, which can meet the requirement of indoor lighting purpose. To the best of our knowledge, the EQEs achieved represent the highest reported to date among hybrid WOLEDs of single- or multi-EML possessing such high CRI. This performance can be comparable to or even higher than some of the high-performance all phosphor-doped WOLEDs demonstrated before.[17a,17b,18] Encouraged by the outstanding EL performance, we subsequently performed a detailed study on the intrinsic working mechanism of this unique device.

3.4 Influence of 4P-NPD on the charge carrier transport

Doping of a guest emitter into a host material may significantly alter charge carrier transport behaviors in EML,[19] in other words, the guest emitter may participate in charge transport, serving as charge carrier trapping sites, or offering new carrier transport channel such as carrier hopping among the emitter sites, especially at high doping concentrations. Since the optimal doping concentration of 4P-NPD in the blue EML is as high as 50 wt%, it is noteworthy to investigate the influence of 4P-NPD doping on the EL performance to understand the excitonic and electronic behaviors.

Firstly, hole- and electron-only devices were fabricated. The hole-only device consists of the following structure: ITO / MoO_3 (10 nm) / NPB (25 nm) / TCTA (5 nm) / CBP: 6 wt% $Ir(ppy)_3$ (6 nm) / CBP (4 nm) / CBP: 3 wt% $Ir(MDQ)_2(acac)$ (5 nm) / CBP: x wt% 4P-NPD (x = 0, 4, 33, 50) (40 nm) / MoO_3 (10 nm) / Al, while the electron-only device contains the following layers: Al / Cs_2CO_3 / TmPyPb (20 nm) / CBP: x wt% 4P-NPD (x = 0, 4, 33, 50) (40 nm) / TmPyPb (20 nm) / TmPyPb: 4 wt% Cs_2CO_3 (20 nm) / Cs_2CO_3 / Al. Figure 3 shows the current density versus applied voltage characteristics of these devices, the hole current density decreased, meaning 4P-NPB as hole trapper, while the electron current density unchanged, indicating the electrons to be directly injected to 4P-NPB, with increasing concentration of 4P-NPD. Therefore, it can be deduced that the current should decrease with increasing concentration of 4P-NPD in hybrid WOLED.

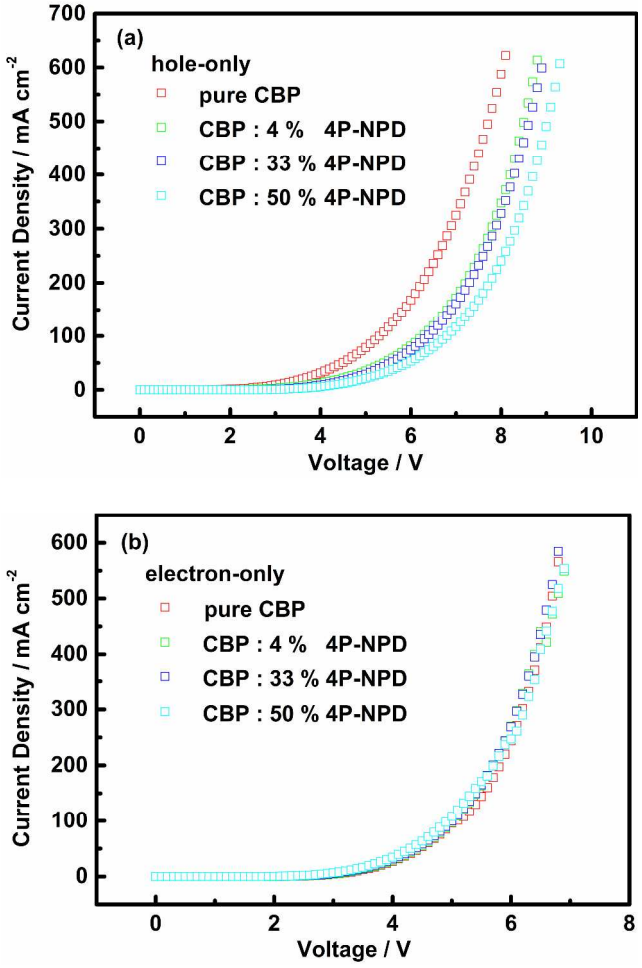

Figure 3. (a): Current density–voltage characteristics of the hole-only devices. (b): Current density–voltage characteristics of the electron-only devices.

To determine the influence of 4P-NPD doping on transport behavior in the EL process, four devices are fabricated by changing the doping concentration of 4P-NPD from 0, to 4, to 33, to 50 wt% while keeping all other parameters of the device unchanged in the hybrid WOLED to allow optimum comparability. Interestingly, the result of current-density-voltage (J-V) characteristics contradicts our assumption. As shown in Figure 4, the increase of current density with increasing concentration of 4P-NPD indicates that the higher concentration of 4P-NPD can facilitate the carrier transport in the CBP host. Taking the differences in the J–V performances into account and incorporating with the results of the hole- and electron-only devices, we could deduce that the electron transport within the emission layer occurs via hopping between 4P-NPD molecule sites.

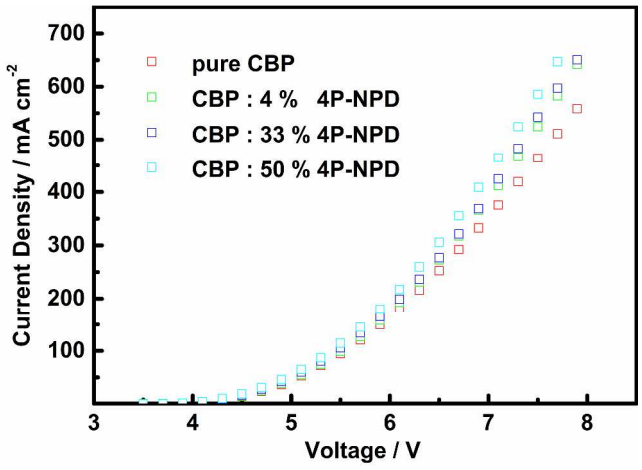

Figure 4. Current density–voltage characteristics as a function of doping concentrations in hybrid WOLEDs.

As mentioned, CBP favors the passage of holes over that of electrons, and the large energy barrier of 0.8 eV between CBP and TmPyPb can prevent holes from being injected into the TmPyPb layer effectively.[20,21a] In addition, as previously established, 4P-NPD doped in CBP can act as hole traps in the blue EML, causing holes to predominantly reside on them. Both aspects make holes accumulate in the blue EML, which can facilitate electron injection into the blue EML via the LUMO of 4P-NPD.[21] Thus, increasing 4P-NPD concentration, which induces a strong hole accumulation in the blue EML, would succeed in further enhancing the built-in electrical field and strengthening the band bending near the interface, which can help with more electrons injection from the cathode side and thus promote their transport. Besides, the hopping distance between neighboring 4P-NPD molecules also affects the electron transport. Increasing the concentration of 4P-NPD will reduce the hopping distance,[5c] and thus further enhance the electron current in the device. In other words, electrons can get favorable hopping sites for conduction due to the short hopping distance. So, a higher concentration of 4P-NPD leads to improved electron injection and transport.

Note that the process of electron transport via hopping on the LUMO of emitter molecule sites can even take place if the LUMO of 4P-NPD is higher than that of CBP, because the LUMO of 4P-NPD is shifted downwards by reduced electron–electron repulsion when the molecule is positively charged.[21d] Therefore, it can conclude that 4P-NPD doped in CBP not only serves as hole traps to retard the hole transport, but also plays the role of an electron-transporting channel. Thus, the increase of current density with increasing 4P-NPD concentration should originate from the enhancement of electron current.

The trapped holes could form 4P-NPD cations, which can recombine with the transported electrons to form excitons directly on 4P-NPD sites. Besides, as just mentioned, 4P-NPD plays the role of an electron-transporting channel and the higher concentration of 4P-NPD causes a better electron hopping on the emitter molecule sites into the blue EML. Therefore, it can be inferred that increasing the concentration of 4P-NPD would result in more excitons generated deep inside the blue EML, widening the exciton formation region. In order to prove this assumption, we fabricated a series of devices by varying the concentration of 4P-NPD in CBP from 0 to 5 to 33 to 50 wt% (see Figure 5). A sensing layer consisting of 3 wt% $Ir(MDQ)_2(acac)$ doped into CBP was incorporated adjacent to the anode side of blue EML. TmPyPb:4 wt% PO-01 was chosen as another sensing layer, which was located at the opposite side of blue EML. The employment of PO-01 is because its primary emission peak at around 560 nm is easily distinguishable from the 4P-NPD and $Ir(MDQ)_2(acac)$ emissions. Due to the fact that $Ir(MDQ)_2(acac)$ (2.0 eV) has a lower triplet energy level than the blue (2.3 eV) and yellow (2.2 eV) emitters,[6,22] it can efficiently absorb triplet excitons generated in the blue EML which originally contributes to the yellow emission, if the exciton generation zone extends into the blue emitting region. In other words, the higher concentration of 4P-NPD, the more likely is the transfer of excitons from 4P-NPD to $Ir(MDQ)_2(acac)$, which can be seen from the EL spectrum where yellow emission decreases whereas orange emission increases. To derive the evidence, we measured the orange and yellow emission peak intensities of each device at the same current density (33.62 mA cm^{-2}). As shown in Figure 5, a higher concentration of 4P-NPD indeed leads to more orange emission with respect to its lower counterpart in the series of devices, providing a strong experimental evidence for the above assumption. It can conclude that higher concentration of 4P-NPD broadens the major exciton formation region.

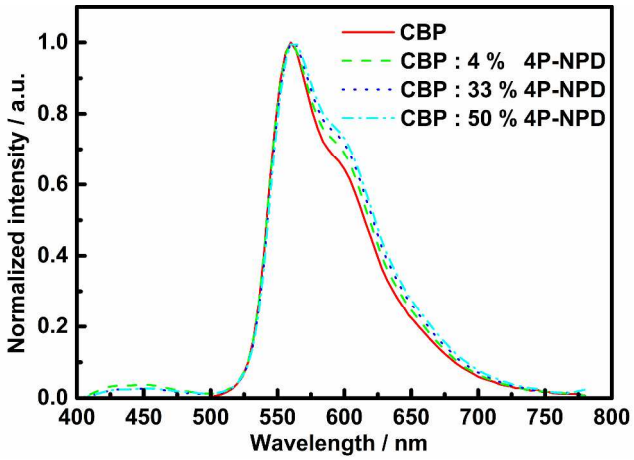

Figure 5. Normalized electroluminescence spectra at a current density of 33.62 mA cm^{-2} for four devices with the structure of ITO / PEDOT / NPB (15 nm) / TCTA (5 nm) / CBP: 3 wt% $Ir(MDQ)_2(acac)$ (3 nm) / CBP: x wt% 4P-NPD (x = 0, 4, 33, 50) (8 nm) / TmPyPb: 4 wt% PO-01 (3 nm) / TmPyPb (12 nm) / n-ETL / Al

3.5 Role of the CBP interlayer

Except for the influence of 4P-NPD on the charge carrier transport, another important element of the novel structure is the introduction of pristine CBP interlayer, which is critical to precisely controlling the distribution of excitons in the emission zone. An undoped CBP interlayer is inserted in the EML, forming a spacer between the green and red regions. This interlayer is employed to avoid exciton quenching on $Ir(ppy)_3$ (2.4 eV) by

$Ir(MDQ)_2(acac)$ molecules which provide lower triplet energy level (2.0 eV), maintaining the balanced white light. To demonstrate the importance of interlayer, device W1 without CBP interlayer was fabricated and its performance was compared to that of the optimized device. Apart from eliminating of the interlayer, all other parameters of deviceW1 were kept unchanged to allow optimum comparability. It is remarkable that the spectrum of device W1 strongly differs from that of the optimized device, as shown in Figure 6. There is nearly no green emission in device W1. This is because most of the excitons in the green region were transferred to the triplet states of orange phosphor, leading to an overwhelmed orange emission with respect to the green emission, such that the EL spectrum is not balanced to reach the white region. However, in the optimized structure, triplet diffusion to $Ir(MDQ)_2(acac)$ is prevented due to the high triplet energy level of interlayer, allowing for an acceptable balanced white light over the operation range of driving voltage.

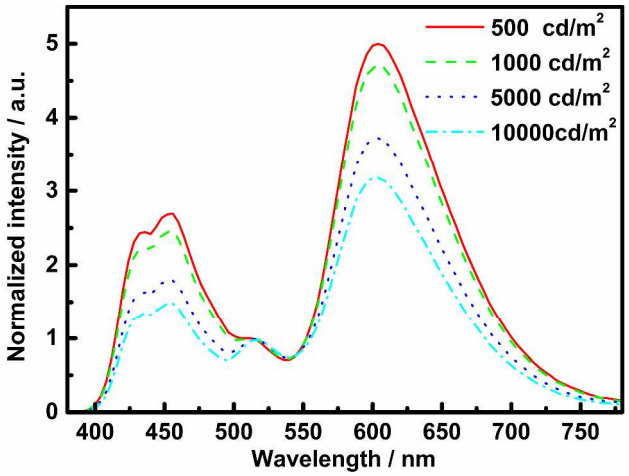

Figure 6. The normalized EL spectra at different brightness levels for device W1 with the structure of ITO / PEDOT / NPB (15 nm) / TCTA (5 nm) / CBP: 6 wt% $Ir(ppy)_3$ (3 nm) / CBP: 3 wt% $Ir(MDQ)_2(acac)$ (2.5 nm) / CBP: 50 wt% 4P-NPD (8 nm) / TmPyPb (12 nm) / n-ETL / Al

On the premise of ensuring an acceptable quality of white light, we prepared other two pairs of devices without the interlayer, those were, device W2 with extremely low $Ir(MDQ)_2(acac)$ concentration (0.5 wt%) while much thicker green EML (10 nm) for device W3,[23] to investigate the feasibility of eliminating the interlayer. Figure 7 (a) and (b) show the EL spectra of device W2 and device W3. It is clearly seen that device W2 and W3 can emit white light, indicating that energy transfer of $Ir(ppy)_3$ triplet excitons to the CBP:$Ir(MDQ)_2(acac)$ layer were frustrated for both devices. However, as shown in Figure 7 (c) and (d), where the efficiency vs. luminance curves of both devices were compared to the optimized device. It can be seen that the device EQE shows a stronger efficiency roll-off for the device W2 compared to the optimized device. One possible explanation is that the low doping level of $Ir(MDQ)_2(acac)$ makes the phosphors not able to take up all the triplet excitons delivered from 4P-NPD, resulting in triplet exciton losses. On the contrary, the optimized device with higher doping level of $Ir(MDQ)_2(acac)$ provides enough red emissive sites, allowing for a nearly complete utilization of triplet energy transferred from 4P-NPD. Although there is not obvious difference on EQE data between the device W3 and the optimized device, especially at high brightness. The device W3 conspicuously shows lower PE because the thicker green EML can result in a high operating voltage. The CBP interlayer can successfully prevent the unwanted energy transfer from the $Ir(ppy)_3$ molecules to the $Ir(MDQ)_2(acac)$ molecules, resulting in a balanced white light, while maintaining a high device efficiency. Thus, the presence of interlayer is necessary in this novel structure.

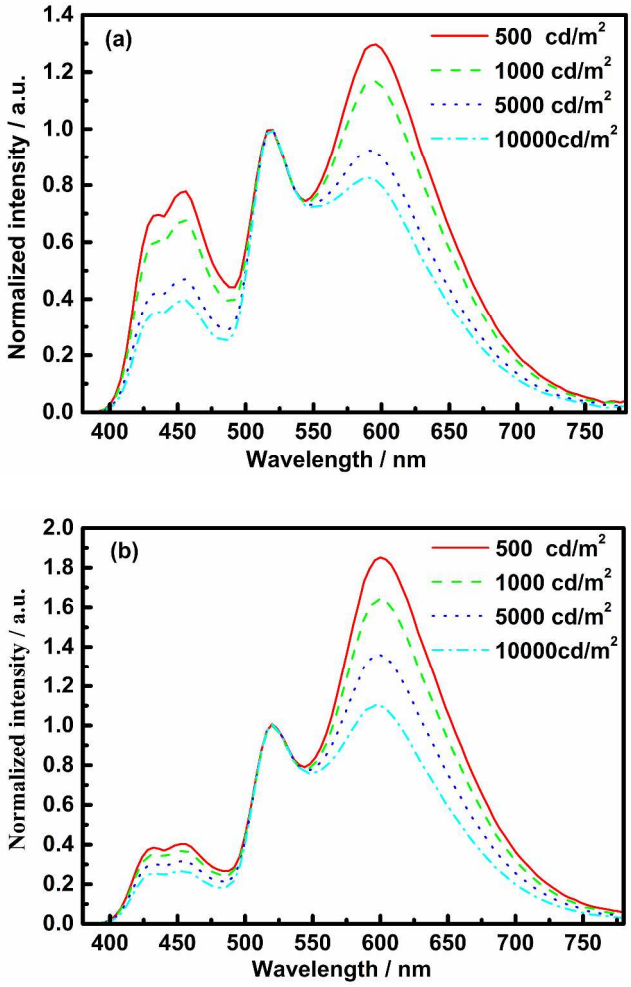

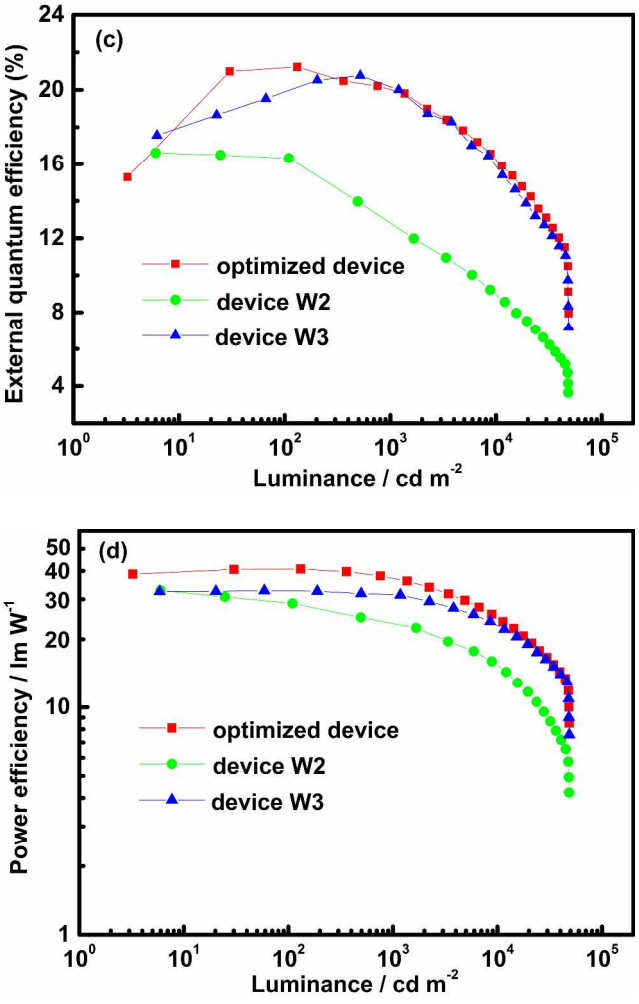

Figure 7. (a) The normalized EL spectra of device W2 at different brightness levels. (b) The normalized EL spectra of device W3 at different brightness levels. (c) External quantum efficiencies of all devices plotted as a function of luminance. (d) Power efficiencies of all devices plotted as a function of luminance.

3.6 Origin of the low efficiency roll-off

Much attention to date has focused on the role of nonradiative quenching processes as the source of efficiency roll-off behavior.[24] The efficiency roll-off processes particularly play a dominant role at large exciton number, i.e., high luminance, to quench the radiative emission of excitons, which detrimentally degrade the device performance for practical applications. According to a previous report by Leo and coworkers,[25] it can be known that triplet-triplet annihilation (TTA) and triplet-polaron quenching (TPQ) are the dominant mechanisms for the efficiency roll-off, both of which are strongly dependent on the local density of excitons. Fortunately, these two effects can be suppressed in the novel structure. Systematic investigations are subsequently performed to unveil the origin of extremely low efficiency roll-off.

As known, CBP shows preferred transport property for holes, causing an overflow of holes in the blue EML. And the large energy offset (0.8 eV) of HOMO between CBP and TmPyPb effectively prevents holes from transporting into the adjacent TmPyPb layer, making the excessive holes prone to accumulate at the interface between the blue EML and the HBL, which would be determinal to the device efficiency by TPQ effect. The large amount of trapped holes on the 4P-NPD sites would reduce the number of accumulated holes at that interface. Alleviating that trend can lower the formation of h+ polarons and thereby limit the quantity of triplet-polaron pairs. Except for that, the high concentration of trapped holes can further assist in electron injection and hence transport via hopping on the emitter molecule sites, which is beneficial to the electron-hole balance. Both aspects are indeed in favor of reduction of the TPQ strength, thus improving the efficiency roll-off.

As proved in the previous section, the major exciton generation zone broadens into the blue EML due to the hole-trapping effect of 4P-NPD, which yields a lower equilibrium triplet exciton density, and reduced the TTA and TPQ behaviors, thus decreasing the efficiency roll-off at high current density. Another question is whether there exists directly exciton generation on the dopants, i.e., direct recombination of carriers on the dopants for green and orange phosphorescences. With this aim, a group of hole- and electron-only devices were fabricated (see Figure 8). Figure 8(a) and (b) shows the current density versus voltage curves of the electron-only devices, significant decrease was found in the current conduction in the CBP layer doped with 3 wt% $Ir(MDQ)_2(acac)$ with respect to that of the pure CBP layer, which indicates that $Ir(MDQ)_2(acac)$ in CBP served as a trapping site for electron, whereas doping 6 wt% $Ir(ppy)_3$ into CBP has almost no influence on electron transport. As shown in Figure 8(d), a decreased hole mobility upon doping of 6 wt% $Ir(ppy)_3$ into CBP than that of the non-doped layer can be observed due to the hole trapping function of $Ir(ppy)_3$. And the hole mobility of a CBP layer doped with 3 wt% $Ir(MDQ)_2(acac)$ was found to be slightly decreased compared to that of the device with an intrinsic 40-nm-thick CBP layer (see Figure 8(c)). Based on the results for the hole- and electron-only devices, direct exciton formation following charge trapping on $Ir(ppy)_3$ and $Ir(MDQ)_2(acac)$ sites indeed contribute to the green and red emissions in the white EL, which is also beneficial to the formation of an extended exciton generation zone, hence decreasing the efficiency roll-off. This exciton generation zone broadening into the green and red EMLs relies on the bipolar transport properties of CBP. Both charge carriers can transport into their own EMLs. Furthermore, from various previous studies on CBP serving as an uniform host for all EMLs, it has been well known that the exciton generation zone is around the both sides of EML, i.e., EBL/EML and EML/HBL,[8b] unlike conventional structures where the exciton generation zone is limited in only one narrow region due to the utilization of "unipolar" electron- or hole-transport host materials. Both processes render a distribution of excitons to form in multiple regions, resulting in further reduction of TTA and TPQ.

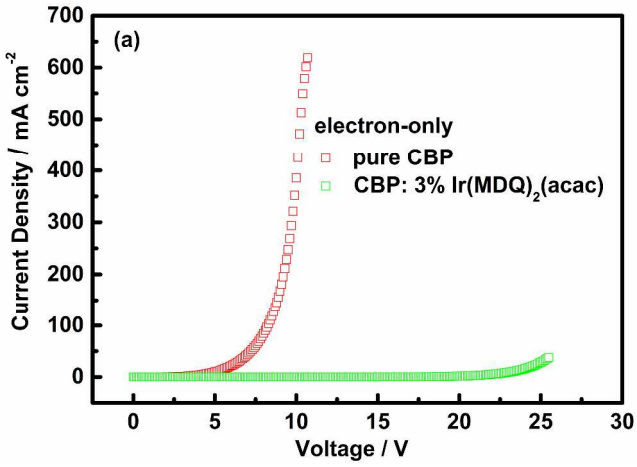

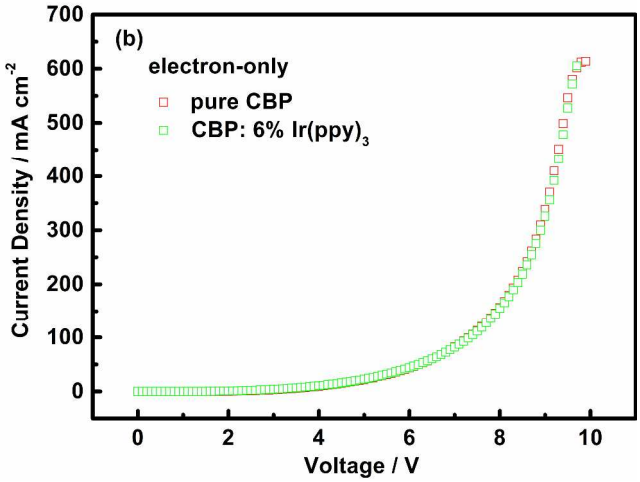

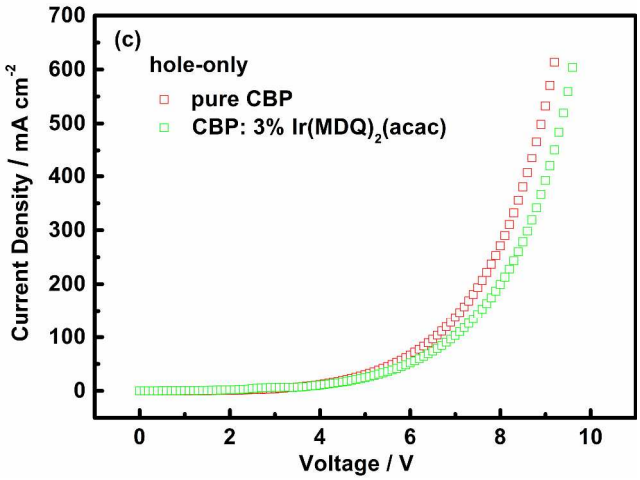

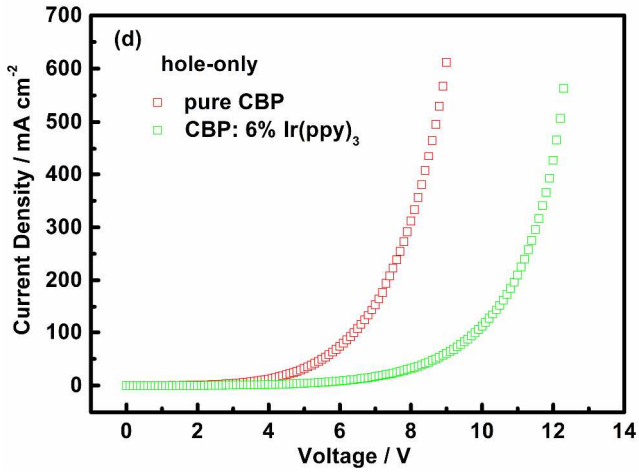

Figure 8. Current-density–voltage characteristics of (a) an electron-only device: AL/LiF (1nm)/TmPyPb (25nm)/undoped CBP or 3 wt% $Ir(MDQ)_2(acac)$ doped CBP (40nm)/CBP:50 wt% 4P-NPD (10nm)/TmPyPb (25nm)/LiF (1nm)/Al, (b) an electron-only device: AL/LiF (1 nm)/TmPyPb (25nm)/undoped CBP or 6 wt% $Ir(ppy)_3$ doped CBP (40nm)/CBP (10nm)/TmPyPb (25nm)/LiF (1nm)/Al, (c) an hole-only device: ITO/MoO_3 (10nm)/NPB (25nm)/TCTA (10nm)/ CBP: 6 wt% $Ir(ppy)_3$ (3nm)/CBP (2nm)/undoped CBP or 3 wt% $Ir(MDQ)_2(acac)$ doped CBP (40nm)/MoO_3 (10nm)/Al, (d) an hole-only device: ITO/MoO_3 (10nm)/NPB (30nm)/TCTA (10nm)/undoped CBP or 6 wt% $Ir(ppy)_3$ doped CBP (40nm)/MoO_3 (10nm)/Al.

3.7 Origin of the color-shift

As shown in Figure 2(c), it is noted that the blue and red emissions decrease simultaneously. The phenomena can be attributed to the change of exciton generation zone with voltage. As known, the exciton formation on the host located in the middle region of EML is negligible, the exciton generation zone should be around the both sides of EML, i.e., EBL/EML and EML/HBL.[7,8b] Due to the imperfect ambipolar transport property of CBP associated with relatively higher hole mobility,[15c,26] at low driving voltages, only a small amount of electrons can be transferred into the green EML and combine with the holes to form excitons which are then available for $Ir(ppy)_3$ molecules. Meanwhile, the majority of excitons are formed on the other side of EML, where both holes and electrons have significant densities. At this stage, the exciton recombination at the EML/HBL interface dominates, leading to the strong blue and orange emission components. Under high drive voltages, due to the increased electron mobility with the electric field,[12,18a] more electrons can penetrate deeper into the anode side of EML, leading more excitons to form in the green EML. Because more holes are consumed in the green EML before they inject into the orange and blue EMLs, the relative intensities of orange and blue emissions decrease, indicating a shift of the major recombination zone from the anode side of EML towards the cathode side.

To obtain a stable color output, further research is required to develop ambipolar host materials with a similar magnitude of both the electron and hole mobility over large operating voltage ranges and form a stable exciton generation zone, ultimately leading to a rather stable color output.

3.8 Universality of the device structure

To demonstrate the universality of this novel device structure, we introduced another blue fluorescent emitter NPB with a moderate triplet state energy (2.3 eV) to replace 4P-NPD (see Figure 9).[4a] Table 1 summarizes the performance of this device. The lower efficiency exhibited in device based on the same architecture is most likely due to the lower PLQY of NPB.[6] However, the device performance is still comparable to or even better than many other counterpart multi-EML hybrid WOLEDs. This result indicates that our novel structure is quite general and can be directly applied to blue fluorophor with moderate triplet state energy (>2.0 eV) even though the PLQY of used blue fluorophor is not high enough.

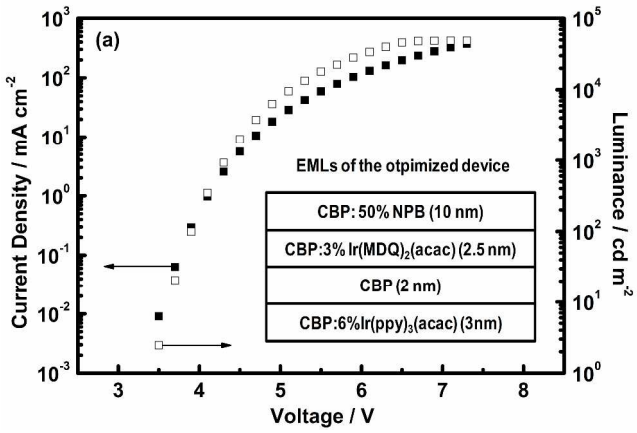

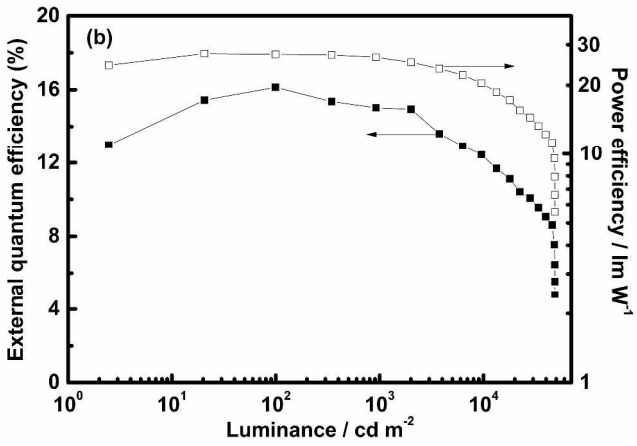

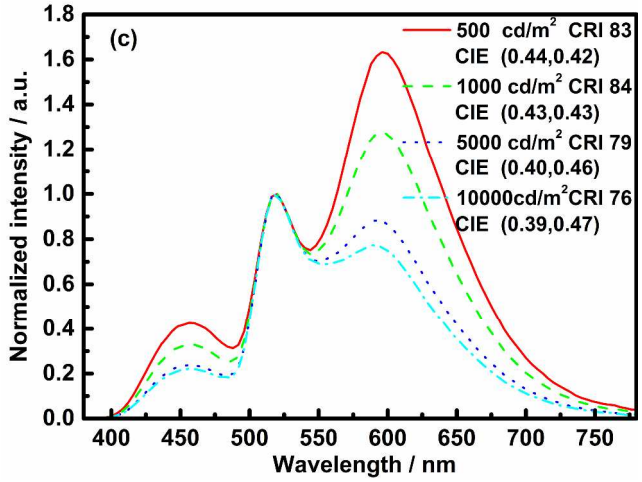

Figure 9. (a): Current density–luminance–voltage characteristics, with luminance measured in forward direction without outcoupling enhancement techniques. The inset shows the components of the EMLs. (b): External quantum efficiency and power efficiency versus luminance characteristics of the device. (c): Normalized EL spectra at different brightness levels.

Table 1.Summary of EL Performance (Forward-Viewing) of the Device S3

EQE [a] [%]	CE [a] [cd A^{-1}]	PE [a] [lm W^{-1}]	CIE [b]	CRI [b]	J_0 [mA cm^{-2}]
16.1,15.0	36.2,36.2	27.5,26.3	(0.43,0.43)	84	197

[a] Order of measured value: maximum, then values at 1000 cd m^{-2}. [b] Measured at 1000 cd m^{-2}.

4. Conclusions

A novel device structure is proposed to achieve fluorescence/phosphorescence hybrid WOLEDs with EQE above 20%. The key features of our novel structure are appropriate utilization of high-efficiency blue fluorophor with moderate triplet state energy and employing bipolar CBP as the host for all EMLs. By virtue of the bipolar transport properties of CBP, both charge carriers can transport into every EMLs, so that the exciton generation zone is not limited in only one narrow region. The distribution of excitons to form in multiple regions, on one hand, provides more flexibility for the arrangement of three (primary-color) EMLs, and hence successfully separating dyes with mismatched triplet energy levels which makes it possible to achieve nearly 100% exciton harvesting, on the other hand, broadens the exciton generation zone, and thus achieving a rather small efficiency roll-off at high current density. The hybrid device shows excellent EL performance with forward-viewing maximum EQE, CE and PE of 21.2%, 49.6 cd A^{-1} and 40.7 lm W^{-1}, then slightly decreases to 20.0%, 49.5 cd A^{-1} and 37.1 lm W^{-1} at 1000 cd m^{-2}. This highly efficient hybrid WOLED based on this universal structure sheds a light on the class of highly efficient blue fluorescent materials with a moderate triplet state energy, thus guiding the design and synthesis of new blue fluorophors. We thereby suggest that for the further development of highly efficient hybrid WOLEDs, it is crucial to consider multiple aspects such as the PLQY of the emitters and the device

structure, rather than focusing exclusively on the triplet state energy of blue fluorophors.

Acknowledgements

The authors gratefully acknowledge the National Natural Science Foundation of China (51333007, 50973104), Ministry of Science and Technology of China (973 program No. 2013CB834805), the Foundation of Jilin Research Council (2012ZDGG001, 20130206003GX, 201105028), and CAS Instrument Project (YZ201103) for the support of this research.

Notes and references

State Key Laboratory of Polymer Physics and Chemistry, Changchun Institute of Applied Chemistry, University of Chinese Academy of Sciences, Changchun 130022, People's Republic of China.
E-mail: mdg1014@ciac.jl.cn

† Electronic Supplementary Information (ESI) available: [details of any supplementary information available should be included here]. See DOI: 10.1039/b000000x/

‡ Footnotes should appear here. These might include comments relevant to but not central to the matter under discussion, limited experimental and spectral data, and crystallographic data.

1. (a) H. B. Wu, L. Ying, W. Yang, and Y. Cao, *Chem. Soc. Rev.*, 2009, **38**, 3391; (b) Z. B. Wang, M. G. Helander, J. Qiu, D. P. Puzzo, M. T. Greiner, Z. M. Hudson, S. Wang, Z. W. Liu, and Z. H. Lu, *Nat. Photon.*, 2011, **5**, 753; (c) M. A. McCarthy, B. Liu, E. P. Donoghue, I. Kravchenko, D. Y. Kim, F. So, and A. G. Rinzler, *Science*, 2011, **332**, 570.
2. (a) C.-H. Chen, W.-S. Huang, M.-Y. Lai, W.-C. Tsao, J. T. Lin, Y.-H. Wu, T.-H. Ke, L.-Y. Chen, and C.-C. Wu, *Adv. Funct. Mater.*, 2009, **19**, 2661; (b) O. Fadhel, M. Gras, N. Lemaitre, V. Deborde, M. Hissler, B. Geffroy, and R. Réau, *Adv. Mater.*, 2009, **21**, 1261; (c) J. Ye, C.-J. Zheng, X.-M. Ou, X.-H. Zhang, M.-K. Fung, and C.-S. Lee, *Adv. Mater.*, 2012, **24**, 3410; (d) C.-J. Zheng, J. Wang, J. Ye, M.-F. Lo, X.-K. Liu, M.-K. Fung, X.-H. Zhang, and C.-S. Lee, *Adv. Mater.*, 2013, **25**, 2205; (e) Y. Tao, Q. Wang, Y. Shang, C. Yang, L. Ao, J. Qin, D. Ma, and Z. Shuai, *Chem. Commun.*, 2009, 77; (f) P.-I Shih, C.-F. Shu, Y.-L. Tung, and Y. Chi, *Appl. Phys. Lett.*, 2006, **88**, 251110; (g) X. Yang, S. Zheng, R. Bottger, H. S. Chae, T. Tanaka, S. Li, A. Mochizuki, and G. E. Jabbour, *J. Phys. Chem. C*, 2011, **115**, 14347; (h) Y. Yang, T. Peng, K. Ye, Y. Wu, Y. Liu, and Y. Wang, *Org. Electron.*, 2011, **12**, 29.
3. (a) M. E. Kondakova, J. C. Deaton, T. D. Pawlik, D. J. Giesen, D. Y. Kondakov, R. H. Young, T. L. Royster, D. L. Comfort, and J. D. Shore, *J. Appl. Phys.*, 2010, **107**, 014515; (b) U. S. Bhansali, H. Jia, M. A. Q. Lopez, B. E. Gnade, W.-H. Chen, and M. A. Omary, *Appl. Phys. Lett.*, 2009, **94**, 203501; (c) C.-L. Ho, W.-Y. Wong, Q. Wang, D. Ma, L. Wang, and Z. Lin, *Adv. Funct. Mater.*, 2008, **18**, 928; (d) B.-P. Yan, C. C. C. Cheung, S. C. F. Kui, H.-F. Xiang, V. A. L. Roy, S.-J. Xu, and C.-M. Che, *Adv. Mater.*, 2007, **19**, 3599; (e) X. Yang, Y. Zhao, X. Zhang, R. Li, J. Dang, Y. Li, G. Zhou, Z. Wu, D. Ma, W.-Y. Wong, X. Zhao, A. Ren, L. Wang, and X. Hou, *J. Mater. Chem.*, 2012, **22**, 7136; (f) P. Chen, W. Xie, J. Li, T. Guan, Y. Duan, Y. Zhao, S. Liu, C. Ma, L. Zhang, and B. Li, *Appl. Phys. Lett.*, 2007, **91**, 023505; (g) J. H. Seo, J. H. Seo, J. H. Park, Y. K. Kim, J. H. Kim, G. W. Hyung, K. H. Lee, and S. S. Yoon, *Appl. Phys. Lett.*, 2007, **90**, 203507; (h) C.-L. Ho, M.-F. Lin, W.-Y. Wong, W.-K. Wong, and C. H. Chen, *Appl. Phys. Lett.*, 2008, **92**, 083301.
4. (a) G. Schwartz, S. Reineke, T. C. Rosenow, K. Walzer, and K. Leo, *Adv. Funct. Mater.*, 2009, **19**, 1319; (b) Y. Divayana, S. Liu, A. K. K. Kyaw, and X. W. Sun, *Org. Electron.*, 2011, **12**, 1; (c) F. Zhao, Z. Zhang, Y. Liu, Y. Dai, J. Chen, and D. Ma, *Org. Electron.*, 2012, **13**, 1049; (d) F. Zhao, N. Sun, H. Zhang, J. Chen, and D. Ma, *J. Appl. Phys.*, 2012, **112**, 084504; (e) J. H. Seo, I. H. Park, G. Y. Kim, K. H. Lee, M. K. Kim, S. S. Yoon, and Y. K. Kim, *Appl. Phys. Lett.*, 2008, **92**, 183303; (f) G. Schwartz, K. Fehse, M. Pfeiffer, K. Walzer, and K. Leo, *Appl. Phys. Lett.*, 2006, **89**, 083509; (g) K. S. Yook, S. O. Jeon, J. Y. Lee, K. H. Lee, Y. S. Kwon, S. S. Yoon, and J. H. Yoon, *Org. Electron.*, 2009, **10**, 1378.
5. (a) M. A. Baldo, D. F. O'Brien, Y. You, A. Shoustikov, S. Sibley, M. E. Thompson, and S. R. Forrest, *Nature*, 1998, **395**, 151; (b) M. A. Baldo, M. E. Thompson, and S. R. Forrest, *Nature*, 2000, **403**, 750; (c) C. Adachi, M. A. Baldo, M. E. Thompson, and S. R. Forrest, *J. Appl. Phys.*, 2001, **90**, 5048; (d) L. X. Xiao, S. J. Su, Y. Agata, H. L. Lan, and J. Kido, *Adv. Mater.*, 2009, **21**, 1271; (e) N. C. Greenham, R. H. Friend, and D. D. C. Bradley, *Adv. Mater.*, 1994, **6**, 491; (f) J. S. Kim, P. K. H. Ho, N. C. Greenham, and R. H. Friend, *J. Appl. Phys.*, 2000, **88**, 1073; (g) Y.-L. Tung, S.-W. Lee, Y. Chi, Y.-T. Tao, C.-H. Chien, Y.-M. Cheng, P.-T. Chou, S.-M. Peng and C.-S. Liu, *J. Mater. Chem.*, 2005, **15**, 460.
6. G. Schwartz, M. Pfeiffer, S. Reineke, K. Walzer, and K. Leo, *Adv. Mater.*, 2007, **19**, 3672.
7. C.-J. Zheng, J. Wang, J. Ye, M.-F. Lo, X.-K. Liu, M.-K. Fung, X.-H. Zhang, and C.-S. Lee, *Adv. Mater.*, 2013, **25**, 2205.
8. (a) B. W. D'Andrade, R. J. Holmes, and S. R. Forrest, *Adv. Mater.*, 2004, **16**, 624; (b) Y. Sun, N. C. Giebink, H. Kanno, B. Ma, M. E. Thompson, and S. R. Forrest, *Nature*, 2006, **440**, 908; (c) E. L. Williams, K. Haavisto, J. Li, and G. E. Jabbour, *Adv. Mater.*, 2007, **19**, 197.
9. N. Sun, Q. Wang, Y. Zhao, Y. Chen, D. Yang, F. Zhao, J. Chen, and D. Ma, *Adv. Mater.*, 2014, **26**, 1617.
10. J. Y. Lee, *Mol. Cryst. Liq. Cryst.*, 2009, **498**, 131.
11. a) M. A. Baldo, D. F. O'Brien, M. E. Thompson, and S. R. Forrest, *Phys. Rev. B*, 1999, **60**, 14422; (b) M. C. Gather, A. Köhnen, and K. Meerholz, *Adv. Mater.*, 2011, **23**, 233; (c) S.R. Forrest, D.D.C. Bradley, and M.E. Thompson, *Adv. Mater.*, 2003, **15**, 1043.
12. Q. Wang, C.-L. Ho, Y. Zhao, D. Ma, W.-Y. Wong, and L. Wang, *Org. Electron.*, 2010, **11**, 238.
13. H. I. Baek, and C. H. Lee, *J. Phys. D: Appl. Phys.*, 2008, **41**, 105101.
14. Q. Wang, and D. Ma, *Chem. Soc. Rev.*, 2010, **39**, 2387.
15. (a) H.-H. Chou, and C.-H. Cheng, *Adv. Mater.*, 2010, **22**, 2468; (b) K.-K. Kim, B.-S. Moon, C.-S. Ha, *J. Appl. Phys.*, 2006, **100**, 064511; c) N. Matsusue, Y. Suzuki, H. Naito, *Jpn. J. Appl. Phys.*, 2005, **44**, 3691.
16. M. A. Baldo, C. Adachi, and S. R. Forrest, *Phys. Rev. B*, 2000, **62**, 10967.
17. (a) S.-J. Su, E. Gonmori, H. Sasabe, and J. Kido, *Adv. Mater.*, 2008, **20**, 4189; (b) H. Sasabe, J. Takamatsu, T. Motoyama, S. Watanabe, G. Wagenblast, N. Langer, O. Molt, E. Fuchs, C. Lennartz, and J. Kido, *Adv. Mater.*, 2010, **22**, 5003.
18. (a) Y.-L. Chang, Y. Song, Z. Wang, M. G. Helander, J. Qiu, L. Chai, Z. Liu, G. D. Scholes, and Z. Lu, *Adv. Funct. Mater.*, 2013, **23**, 705; (b) H. Huang, X. Yang, B. Pan, L. Wang, J. Chen, D. Ma and C. Yang, *J. Mater. Chem.*, 2012, **22**, 13223; (c) M.-S. Lin, L.-C. Chi, H.-W. Chang, Y.-H. Huang, K.-C. Tien, C.-C. Chen, C.-H. Chang, C.-C. Wu, A. Chaskar, S.-H. Chou, H.-C. Ting, K.-T. Wong, Y.-H. Liu and Y. Chi, *J. Mater. Chem.*, 2012, **22**, 870; (d) L. Duan, D. Zhang, K. Wu , X. Huang, L. Wang, Y. Qiu, *Adv. Funct. Mater.*, 2011, **21**, 3540; (e) B. Pan, B. Wang, Y. Wang, P. Xu, L. Wang, J. Chen and D. Ma, *J. Mater. Chem. C*, 2014, **2**, 2466; (f) Y. H. Son, Y. J. Kim, M. J. Park, H.-Y. Oh, J. S. Park, J. H. Yang, M. C. Suh and J. H. Kwon, *J. Mater. Chem. C*, 2013, **1**, 5008.
19. (a) Y. Liu, L.-S. Cui, M.-F. Xu, X.-B. Shi, D.-Y. Zhou, Z.-K. Wang, Z.-Q. Jiang and L.-S. Liao, *J. Mater. Chem. C*, 2014, **2**, 2488; (b) S.-C. Dong, Y. Liu, Q. Li, L.-S. Cui, H. Chen, Z.-Q. Jiang and L.-S. Liao, *J. Mater. Chem. C*, 2013, **1**, 6575; (c) W.-C. Lin, W.-C. Huang, M.-H. Huang, C.-C. Fan, H.-W. Lin, L.-Y. Chen, Y.-W. Liu, J.-S. Lin, T.-C. Chaoc and M.-R. Tsengc, *J. Mater. Chem. C*, 2013, **1**, 6835; (d) M. Cai, T. Xiao, E. Hellerich, Y. Chen, R. Shinar, and J. Shinar, *Adv. Mater.*, 2011, **23**, 3590; (e) C.-H. Fan, P. Sun, T.-H. Su, and C.-H. Cheng, *Adv. Mater.*, 2011, **23** , 2981; (f) L.-S. Cui, Y. Liu, X.-D. Yuan, Q. Li, Z.-Q. Jiang and L.-S. Liao, *J. Mater. Chem. C*, 2013, **1**, 8177; (g) S. O. Jeon, S. E. Jang, Hyo S. Son, and J. Y. Lee,

Adv. Mater., 2011, **23**, 1436; (h) F. Huang, P. I. Shih, C. F. Shu, Y. Chi, and A. K. Y. Jen, *Adv. Mater.*, 2009, **21**, 361.
20. (a) J.-K. Bin, N.-S. Cho, and J.-I. Hong, *Adv. Mater.*, 2012, **24**, 2911; (b) S.-J. Su, T. Chiba, T. Takeda, and J. Kido, *Adv. Mater.*, 2008, **20**, 2125.
21. (a) T. Zheng, and W. C. H. Choy, *Adv. Funct. Mater.*, 2010, **20**, 648; (b) J. Huang, G. Li, E. Wu, Q. Xu, and Y. Yang, *Adv. Mater.*, 2006, **18**, 114; (c) T. W. Lee, *Adv. Funct. Mater.*, 2007, **17**, 3128; (d) G. He, O. Schneider, D. Qin, X. Zhou, M. Pfeiffer, and K. Leo, *J. Appl. Phys.*, 2004, **95**, 5773.
22. (a) J. Wünsche, S. Reineke, B. Lüssem, and K. Leo, *Phys. Rev. B*, 2010, **81**, 245201; (b) J. H. Jou, C. H. Chen, J. R. Tseng, S. H. Peng, P. W. Chen, C. I. Chiang, Y. C. Jou, J. H. Hong, C. C. Wang, C. C. Chen, F. C. Tung, S. H. Chen, Y. S. Wang, and C. L. Chin, *J. Mater. Chem. C*, 2013, **1**, 394.
23. (a) B. W. D'Andrade, M. E. Thompson, and S. R. Forrest, *Adv. Mater.*, 2002, **14**, 147; (b) N. Matsusue, S. Ikame, Y. Suzuki, and H. Naito, *IECIE Trans. Electron.*, 2005, **E87-C**, 2033.
24. (a) L. Deng, J. Li, G.-X. Wang and L.-Z. Wu, *J. Mater. Chem. C*, 2013, **1**, 8140; (b) N. C. Erickson, and R. J. Holmes, *Adv. Funct. Mater.*, 2013, **23**, 5190; (c) D. Song, S. Zhao, and H. Aziz, *Adv. Funct. Mater.*, 2011, **21**, 2311; (d) S. Xue, L. Yao, C. Gu, H. Zhang, F. Shen, Z. Xie, H. Wu and Y. Ma, *J. Mater. Chem. C*, 2013, **1**, 7175; (e) H. Cao, H. Sun, Y. Yin, X. Wen, G. Shan, Z. Su, R. Zhong, W. Xie, P. Lia and D. Zhua, *J. Mater. Chem. C*, 2013, **2**, 2150; (f) R. Tao, J. Qiao, G. Zhang, L. Duan, C. Chen, Liduo Wang, and Y. Qiu, *J. Mater. Chem. C*, 2013, **1**, 6446.
25. S. Reineke, K. Walzer, and K. Leo, *Phys. Rev. B*, 2007, **75**, 125328.
26. J.-W. Kang, S.-H. Lee, H.-D. Park, W.-I. Jeong, K.-M. Yoo, Y.-S. Park, and J.-J. Kim, *Appl. Phys. Lett.*, 2007, **90**, 223508.

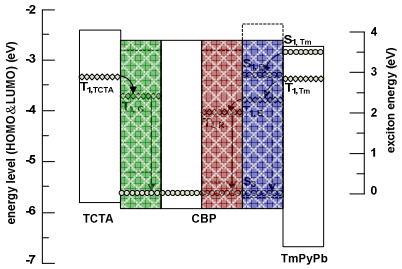

Based on delicate device structure design, a novel (phosphorescence/fluorescence) hybrid WOLED with nearly 100% exciton harvesting is demonstrated.